

A Two Dimensional Laser-Wire Scanner For Electron Accelerators

A. Bosco ^{a,1} M. T. Price ^a G. A. Blair ^a S. T. Boogert ^a
G. Boorman ^a S. Malton ^a C. Driouichi ^{a,2} T. Kamps ^b
F. Poirier ^c K. Balewski ^c E. Elsen ^c V. Gharibyan ^c H-C. Lewin ^c
S. Schreiber ^c N. Walker ^c K. Wittenburg ^c

^a*John Adams Institute for Accelerator Science at Royal Holloway, University of
London, Egham, Surrey TW20 0EX, UK.*

^b*Berliner Elektronenspeicherring - Gesellschaft für Synchrotronstrahlung, Albert
Einstein-Str. 15, 12489 Berlin, Germany.*

^c*Deutsches Elektronen-Synchrotron, Notkestraße 85, 22607 Hamburg, Germany.*

Abstract

A two-dimensional laser-wire scanner capable of measuring the transverse charge profiles of an electron (or positron) bunch has been constructed at the PETRA accelerator in DESY. The development of the system is explained in this paper, along with descriptions of its photon detector and laser system. Results of transverse profile scans are presented for both horizontal and vertical directions, where the measurement error is less than 2.8 % for scan times of less than 50 seconds for the vertical profile scan.

1 Introduction

Laser based beam profile monitors, and in particular the laser-wire (LW), will be needed to measure electron (or positron) beam sizes for future synchrotron light sources [1] and electron-positron colliders [2]. Due to the small emittance and high power requirements of these machines, the use of traditional profiling

¹ Physics Dept. Royal Holloway, University of London, Egham, Surrey, TW20 0EX, UK. Tel: +44(0)1784 41 4304. E-mail: alessio.bosco@rhul.ac.uk

² Present institution: Niels Bohr Institute, Blegdamsvej 17, 2100, Copenhagen, Denmark.

26 methods such as wire scanners or screens is limited [3]. For these reasons,
 27 LWs will be essential to monitor the transverse emittance at future electron
 28 accelerators. The results presented in this paper were obtained using a positron
 29 beam, all the conclusions are also applicable to electron beams.

30 The LW is based on inverse Compton scattering ($e\gamma \rightarrow e\gamma$) between the elec-
 31 trons and laser photons [3]. By counting the number of Compton scattered
 32 photons produced as a function of the laser position, it is possible to recon-
 33 struct the spatial distribution of the electron bunch. Due to the low rate of
 34 the inverse Compton scattering process, the LW is inherently a non invasive
 35 profiling technique [4]. Furthermore, it has a much improved resolution [5],
 36 faster profiling speed [6] and does not suffer from the mechanical issues of
 37 traditional wire scanners.

38 This paper describes the upgrade of the one-dimensional (vertical profiling)
 39 LW tested previously at PETRA [7] to a two-dimensional (2D) bunch profiler,
 40 where the laser beam can be sent to collision in either the horizontal or the
 41 vertical direction alternately, enabling it to perform a vertical profile (VP)
 42 or horizontal profile (HP) measurement, respectively. New capabilities of the
 43 LW, such as electron beam finding, fast scanning and longitudinal scanning
 44 are also discussed. This work is complementary to the R&D currently ongoing
 45 at the accelerator test facility (ATF) at KEK [5], where the emphasis is on
 46 scanning with very small laser spot-sizes.

47 **2 Experimental Setup**

48 Figure 1 shows a plan overview of the LW experimental layout on the east
 49 bending arc of the PETRA ring. It illustrates the major components of the
 50 LW system; high power laser, optical scanning systems, beam position monitor
 51 (BPM) and Compton calorimeter. The laser pulse collides with the positron
 52 bunch within a custom built vacuum vessel with optical view ports for laser
 53 light. The point where the laser light intersects the positron bunch is defined
 54 as the interaction point (IP) which is not fixed but depends on the positron
 55 beam orbit. The Compton photons and charged beam are separated by a
 56 downstream dipole magnet. After separation the Compton photons exit the
 57 PETRA beam pipe through a 6 mm thick Aluminium window before reaching
 58 the calorimeter. The positron beam position is measured using a standard
 59 PETRA four button pick-up BPM.

60 A commercially available Neodymium-doped Yttrium Aluminium Garnet (Nd:YAG)
 61 laser system was used to produce the high power light pulses required for
 62 Compton scattering. The high power laser beam was transported from the
 63 laser hut to the interaction area inside the PETRA tunnel through an exist-

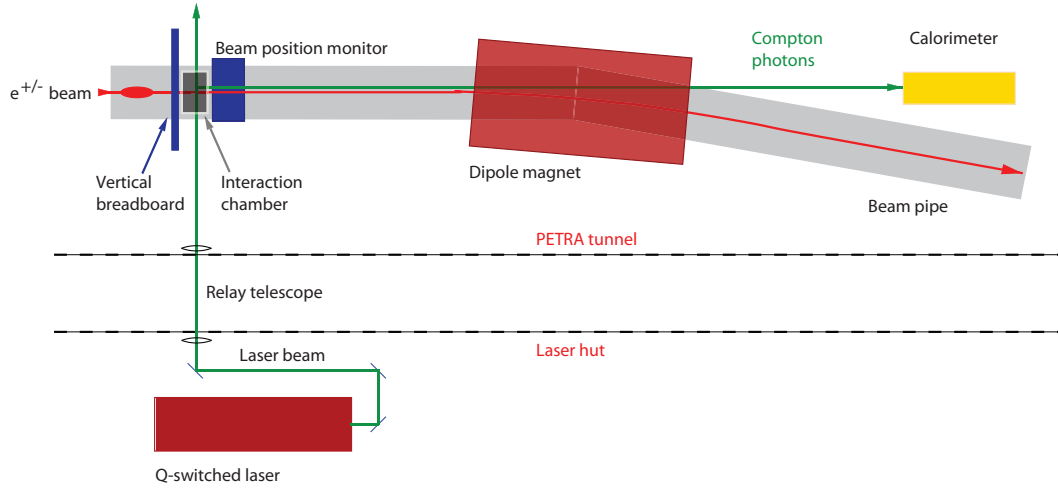


Fig. 1. Overview of the LW setup. A detailed schematic of the vertical breadboard is shown in Fig. 2.

ing access pipe. The total transport distance was about 15 m and the transport optics used a one-to-one imaging Gaussian telescope consisting of two 5 m focal length lenses separated by a 10 m distance. Having passed through the Gaussian telescope arrangement, the laser beam reached the 2-D vertical LW breadboard mounted around the PETRA beam pipe, where it was then guided onto a 3-times magnification beam expander. Fig. 2 shows a schematic illustrating the technical features of the LW optical scanning system, and Fig. 3 shows a photograph of the LW optical scanning system in place on PETRA. The beam expander is configured to increase the laser beam diameter to 25 mm and collimate it. The laser beam is then guided to one of two scanning systems (one for each transverse profile) via the use of a motorized flipping mirror. The scanning systems are identical in design, and are arranged so that one is rotated 90° relative to the other about the IP; a schematic of the vertical scanning system is shown in Fig. 4.

2.1 Scanning System

The scanning systems contain a piezo-driven mirror, to deflect the laser beam, and a commercially available convergent lens (CVI LAP 250) with a focal length of 250 mm, which focuses the beam down to a laser spot size $\sigma_0 = 4.5 \mu\text{m}$, where $\sigma_0 \equiv W_0/2$. The scanning systems are mounted on translation stages to allow movement of the focused laser spot in the transverse plane of the positron bunch, as indicated in Fig. 4. The lens is also mounted on a small translation stage that moves parallel to the axis of laser propagation; this allows the focus position of the laser beam to be changed.

The scanning mirror is a 2 inch multilayer coated mirror (99.9% reflective at

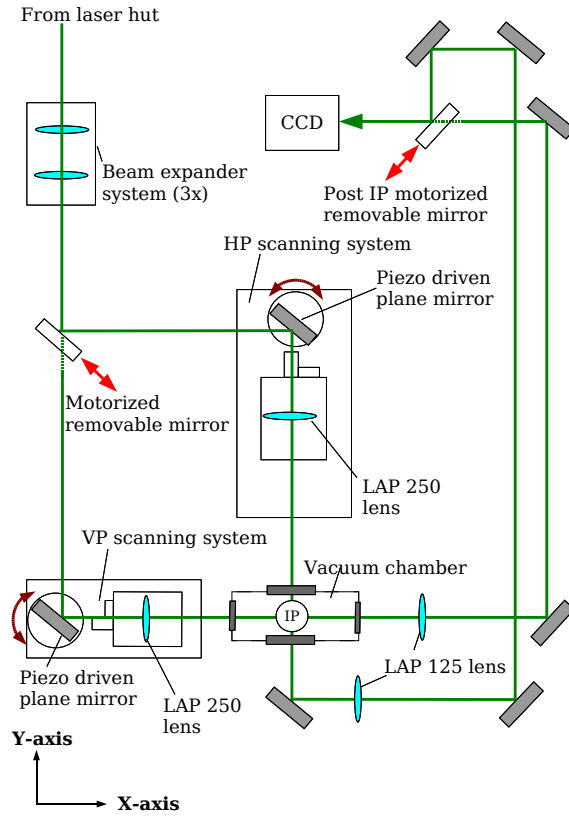


Fig. 2. Schematic of the LW optical scanning system. The x and y axes are normal to the positron beam trajectory. A close up of the VP scanning system is shown in Fig. 4.

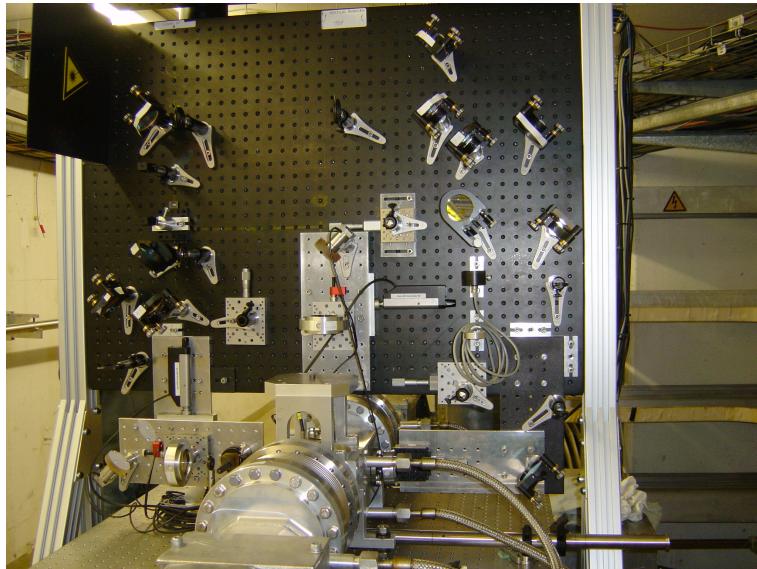


Fig. 3. Photograph of the LW optical scanning system.

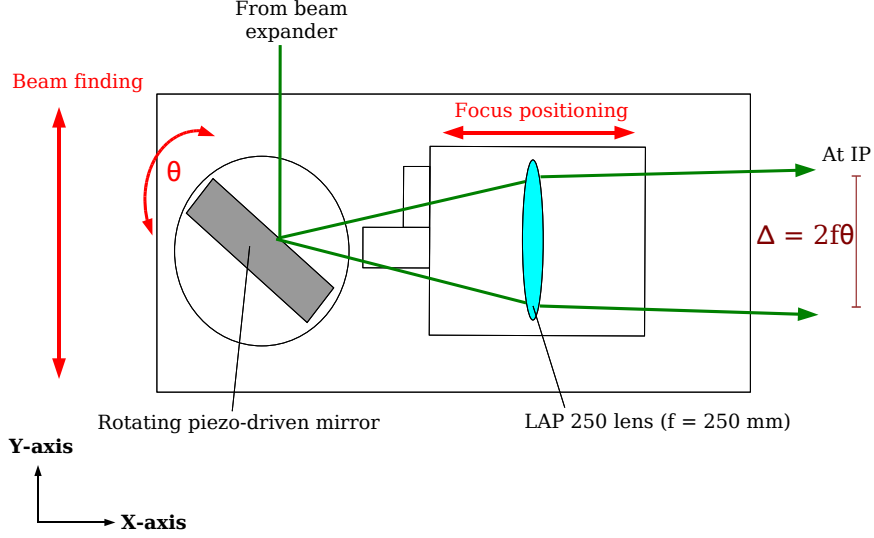


Fig. 4. Schematic of the vertical profile scanning system, which contains the piezo-driven mirror and focusing lens.

532 nm). It is mounted on a piezo-electric stack which can be deflected by a maximum angle of approximately 2.5 mrad (with an applied voltage of 100V). By rotating the piezo-driven mirror by an angle θ the laser beam is steered by an angle 2θ . The shift in transverse position of the focus (Δ) obtained when a laser beam is deflected by angle 2θ at the input of a focusing lens (with focal length f), is given by: $\Delta = 2f\theta$. Given the 250 mm focusing lens and the maximum deflection of 2.5 mrad by the piezo-driven mirror, the total maximum scanning range was 1.25 mm. In addition, the beam finding translation stage can be used for shifting the position of the laser focus; providing a complementary method for scanning larger ranges than permitted by the piezo-electric system.

2.2 Post IP

As the laser beam travels past the IP it becomes divergent and needs to be refocused by a convergent lens (CVI LAP 125) for imaging. The lens has a focal length of $f = 125$ mm and images the plane of the IP on to a CCD camera. The magnification factor of this arrangement is 8.3 and is determined by the ratio of the optical distance between the lens and the CCD camera to the optical distance of the IP to the lens [8,9]. Two such identical post IP imaging systems were constructed, one for each profiling axis. An overview of the optical path from the output of the beam expander to the post IP CCD camera is shown in Fig. 5. An image of the laser intensity profile was taken at the post IP

location, using a laser diagnostic camera (Gentec WinCamD) and is shown in Fig. 6. The analysis indicates that the post IP beam radius $W_M \simeq 75 \mu\text{m}$, which is magnified by the factor of 8.3 discussed above. Therefore the true spot size at the IP is $W_0 \simeq 9 \mu\text{m}$. This is in good agreement with the ABCD matrix calculation shown in Fig. 5.

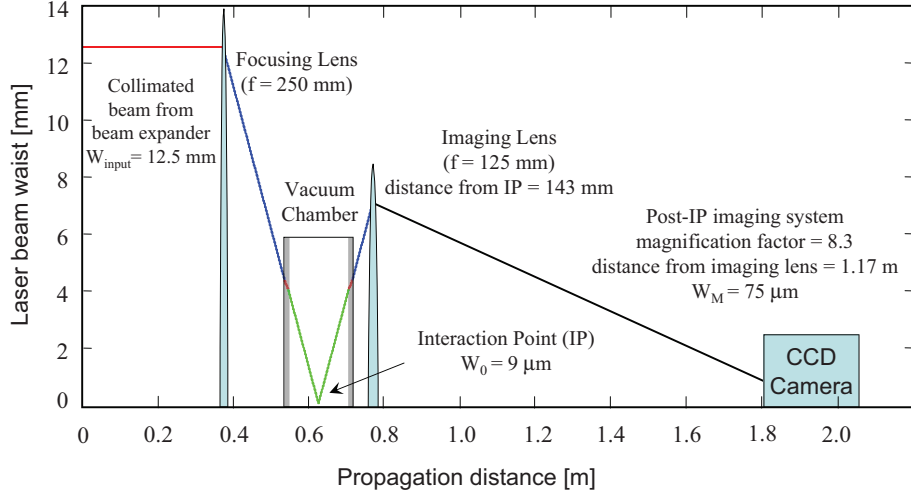


Fig. 5. Plot of the ABCD matrix calculated beam size from the beam expander to the post IP CCD camera, taking into account the mode quality factor of the laser (M^2). W_0 is the laser spot radius as described in section 2.3.1.

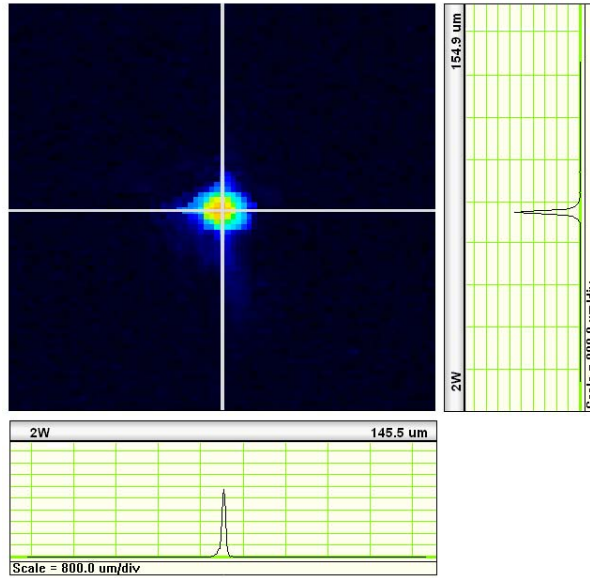


Fig. 6. Laser pulse image taken using CCD profiling equipment in the post IP section of the LW system.

115 The LW laser system must be capable of producing high power light pulses
 116 with good transverse and longitudinal mode quality. The laser system is in-
 117 jection seeded to eliminate longitudinal mode-beating; an effect which creates
 118 temporal sub-structure within the laser pulse at the level of 100 ps. This
 119 is the same order of magnitude as the positron bunch length and therefore
 120 makes beam-size measurement more statistically challenging; the elimination
 121 of mode-beating is thus important for making fast scans [7]. To illustrate the
 122 effect of the seeding process on the longitudinal profile of the laser pulse, scope
 123 traces of the output of a photodiode are shown for the laser system unseeded
 124 and seeded in figures 7 (a) and 7 (b), respectively. A commercially available
 125 injection seeded Q-switched Nd:YAG laser capable of delivering 12 MW light
 126 pulses at 20 Hz was chosen. Such a high power was needed in order to gen-
 127 erate a sufficient number of Compton events per laser pulse as described in
 128 section 3.

129 The fundamental wavelength produced by the Nd:YAG laser is 1064 nm, which
 130 is frequency doubled (using a second harmonic generating crystal) to obtain
 131 a wavelength of 532 nm. This process is not 100 % efficient and the remnant
 132 1064 nm light component is separated using dichroic mirrors and dumped.
 133 Adjustment of the intensity of the laser light was achieved by rotating the
 134 polarization of the laser light relative to a Brewster plate using a half-wave
 135 plate. A summary of the laser characteristics is presented in Table 1.

	Value	Units
Pulse energy at 532 nm	60 ± 5	mJ
Peak power at 532 nm	12 ± 1	MW
Repetition rate	20	Hz
Pulse duration	5 ± 1	ns
RMS pulse jitter (rel. to ext. trigger)	1	ns
Mode quality factor (M^2)	2.68 ± 0.05	
Horizontal angular jitter	18.8	μrad
Vertical angular jitter	9.4	μrad

Table 1
Summary of laser properties.

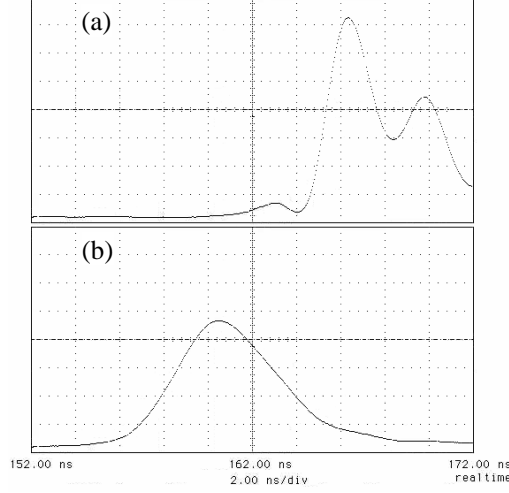


Fig. 7. Oscilloscope trace of the laser pulse as measured by a fast photo-diode (rise time ~ 1 ns) when the laser was unseeded (a) and seeded (b).

2.3.1 Transverse Mode: M^2 Measurements

The laser beam propagates with radius described by the formula:

$$W(z) = W_0 \left[1 + \left(\frac{M^2 \lambda}{\pi W_0^2} \cdot z \right)^2 \right]^{\frac{1}{2}} \quad (1)$$

where $W(z)$ is the laser spot radius (distance from the center of the distribution to the position where the intensity drops by a factor e^{-2}), W_0 is the minimum laser waist, λ is the laser wavelength and M^2 is a factor ≥ 1 which describes the quality of the real beam compared to an ideal TEM_{00} Gaussian beam (for which $M^2 = 1$) [8].

The M^2 of the laser beam was measured by focusing it with a plano-convex lens of focal length 500 mm. CCD images of the laser beam were recorded using the WinCamD at a range of distances from the focusing lens. The beam radius data as a function of camera position are plotted in Fig. 8 and fit using Eqn. 1. The M^2 obtained from the fit was 2.68 ± 0.05 . This value is compatible with the measured waists of $W_{\text{input}} = 12.5$ mm and $W_0 = 9 \mu\text{m}$ using the following formula:

$$W_{\text{input}} W_0 = M^2 \cdot \frac{\lambda f}{\pi} = \text{constant} \quad (2)$$

where λ is the wavelength of the laser light [8]. Given that $W_{\text{input}} = 12.5$ mm, $f = 250$ mm and $\lambda = 532$ nm, Eqn. 2 gives $W_0 \simeq 9 \mu\text{m}$, which is consistent with the post-IP CCD camera measurements described in section 2.2. As $W_0 = 2\sigma$, this gives $\sigma = 4.5 \mu\text{m}$.

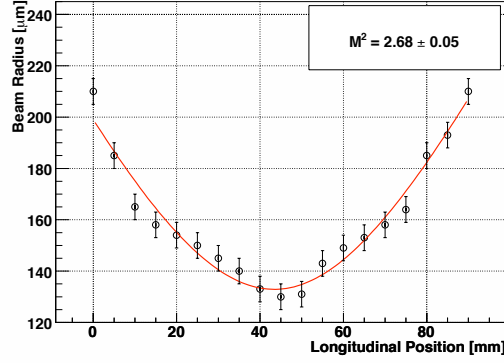


Fig. 8. Measurement of M^2 using a $f = 500$ mm lens. The fit equation is given in Eqn. 1. The fit gives $M^2 = 2.68 \pm 0.05$.

2.3.2 Pointing Jitter Measurement

The laser system produces light pulses with a natural angular jitter, or pointing instability. Knowledge of this jitter is required in order to determine the contribution of such an effect to beam size measurements. In order to determine its pointing stability, the laser was focused using a 1 m focal length lens onto an industrial digital camera (with pixel size $6.7 \mu\text{m}$) and successive laser shots were measured. To create a pedestal, 100 images were taken of the ambient light (no laser) and averaged. This was subtracted from each of a further 100 images taken with the laser firing. Each background subtracted image is projected on to the x and y axes and fit to a Gaussian, the fit centroids are plotted in Fig. 9.

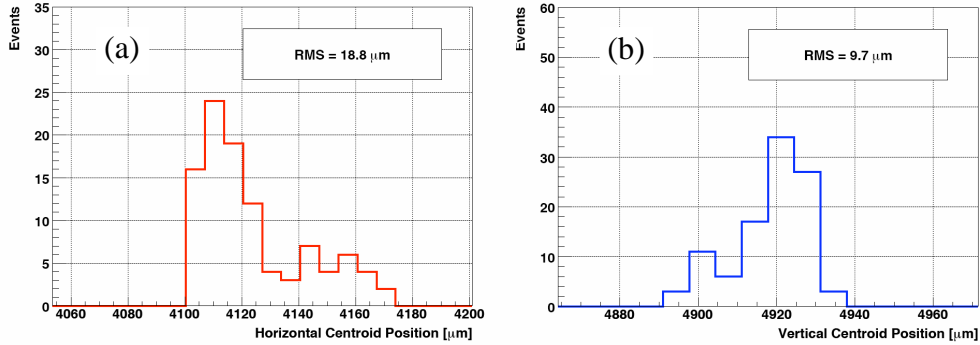


Fig. 9. Histograms showing the distribution of laser spot in the horizontal (a) and vertical (b) axes of the digital camera.

From Fig. 9, the pointing jitter is measured to be $18.8 \mu\text{rad}$ in the horizontal direction and $9.7 \mu\text{rad}$ in the vertical direction. This horizontal angular jitter is transformed by the light transport optics into a position variation at the IP

perpendicular to the direction of the positron beam. The combination of the 3-times magnification telescope and 250 mm focusing lens results in a position jitter, σ_{jitter} , at the IP of $1.6 \mu\text{m}$.

2.3.3 Laser Synchronization

PETRA provides two TTL-level signals for synchronising the laser to the positron bunches, a 96 ns (10.42 MHz) bunch clock and a $7.68 \mu\text{s}$ (130.2 kHz) revolution clock. The timing jitter of the bunch clock and the revolution clock with respect to the BPM signal at the LW IP is negligible compared to the timing jitter of the laser relative to the revolution clock.

A custom designed VME-based trigger card (“LT2”) supplies the laser with a Fire signal, to fire the flash-lamps, and a Q-switch signal that operates the Pockels cell and allows light out of the laser. A timing overview is shown in Fig. 10. The LT2 trigger card can adjust the revolution clock to Q-switch timing in steps of 0.5 ns to synchronise the laser pulse, of width 5 ns, with the positron bunch. The stability of the LT2 output is dependent upon the stability of the timing signals from PETRA. The Fire to Q-switch time is adjusted using a fast rise-time photodiode to look at the light output of the laser, and the time adjusted until a peak in the output is found, typically of order $182.5 \mu\text{s}$. Both the Fire and Q-switch signals are then adjusted together relative to the revolution clock to synchronise with the positron bunch at the IP.

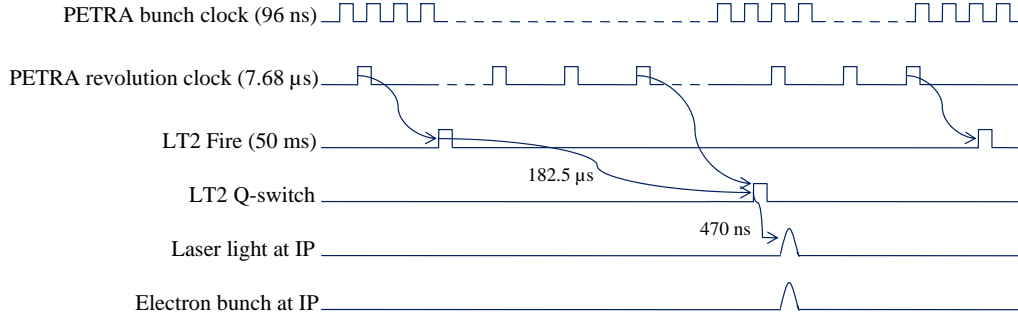


Fig. 10. Schematic summarizing the synchronization signals for the LW DAQ.

2.4 Photon Detector

The photon detector is made of nine lead tungstate crystals organized in a 3×3 matrix. This is optically connected to a photo-multiplier (PMT) which amplifies the output from the lead tungstate crystals. The detector is housed within an arrangement of lead blocks which serves to protect against synchrotron and other low energy radiation.

197 The calorimeter was tested in the DESY Test Beam 24 beam line, and exposed
 198 to single electrons of various energies. The calorimeter voltage output was
 199 recorded on digital sampling oscilloscope for 500 ns triggered just before beam
 200 arrival. A minimum of 10 scope measurements were taken for each particle
 201 energy and PMT voltage setting. The mean peak signal from the PMT was
 202 determined for different beam energies at a fixed PMT voltage of -1115 V.
 203 This is plotted in Fig. 11 and shows that the calorimeter response is linear.
 204 Further details of this work can be found in [9,10]

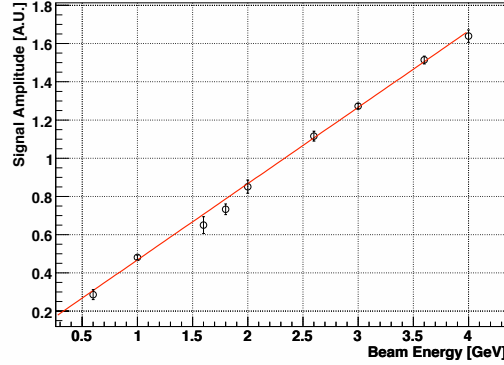


Fig. 11. The mean peak signal from the PMT is plotted against the electron test-beam energy.

205 2.5 The Data Acquisition System

206 An overview of the data acquisition system (DAQ) is shown in Fig. 12. It uses
 207 a National Instruments (NI) M-series high-speed multifunction DAQ card for
 208 the analogue-to-digital and digital-to-analogue conversion (ADC and DAC).
 209 The DAQ software is written using NI LabVIEW, for both the control of the
 210 LW and the online analysis of the data. Customized modules are used for
 211 control of the piezo scanner and calorimeter output conditioning.

212 The DAQ is triggered by a signal from LT2 that has the same timing as Laser
 213 Fire. A counter (CTR0) is triggered by this signal and counts for a specific time
 214 delay, CTR0 delay, after which the CTR0 output goes high for the duration
 215 of the CTR0 pulse, which opens the window for the peak detector, and starts
 216 a second counter (CTR1). CTR1 counts for the CTR1 delay and then rises,
 217 causing the two ADC channels (for the peak detector and the piezo amplifier
 218 monitor) to be read on this edge. When CTR0 falls, this triggers the DAC to
 219 output its next value. The DAQ then resets both counters and waits for the
 220 next Fire signal.

221 The DAQ system also controls the translation stages used for beam-finding

and focus position movement described in section 2.1.

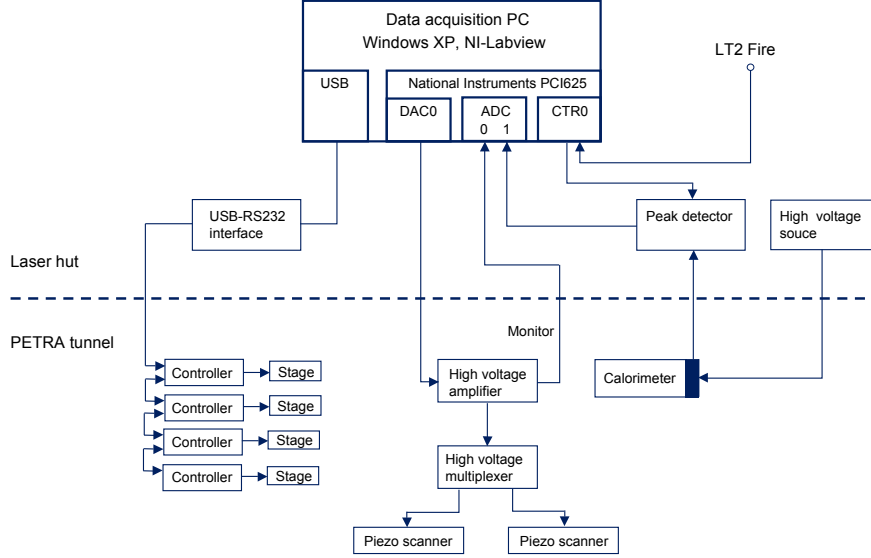


Fig. 12. Schematic of the LW data acquisition system.

3 Data Taking and Results

The following data was taken using PETRA set with the standard HERA injection optics with one positron bunch, at a current of 0.5 mA and a beam energy of 6 GeV. For these beam settings and the laser parameters described in section 2.3, the number of Comptons generated per laser pulse is approximately 1100 for the VP and 120 for the HP [3,9]. The data was taken in dedicated fills, but the LW could also be run parasitically during synchrotron radiation runs for HASYLAB.

The LW can operate two types of scan enabling it to perform bunch size measurements spanning over three orders of magnitude (from 10^{-5} – 10^{-2} m).

- **Ramp scan** - performed by rotating the piezo-driven plane mirror and keeping the beam-finding and focus positioning translation stages fixed. The piezo-driven mirror has a maximum angular scan range of 2.5 mrad, which corresponds to a position shift at the IP of $1250 \mu\text{m}$; which is suitable for positron bunch sizes smaller than $200 \mu\text{m}$.
- **Stage scan** - performed by moving the beam finding translation stage and keeping the piezo-driven mirror and focus positioning translation stage fixed. The stage used for moving the beam-finding translation stage has a maximum scan range of 50 mm and a minimum step size of $1 \mu\text{m}$. This scan type may be used to scan bunch sizes greater than $200 \mu\text{m}$.

243 The position of the laser focus relative to the positron beam can be moved
 244 by the focus positioning translation stage, as explained in section 2.1. Then
 245 either a ramp scan or stage scan may be performed to obtain the positron
 246 beam size.

247 3.1 Profile Measurements

248 This section presents positron bunch size measurements in the vertical and
 249 horizontal axes. An example vertical profile is shown in Fig. 13. This scan
 250 uses 30 laser positions and the signals from 30 laser shots are averaged for
 251 each position. At the laser repetition rate of 20 Hz a scan took 45 seconds to
 252 complete.

253 To extract the measured sigma of the scan, σ_m , the data are fit to the sum
 254 of a Gaussian plus a constant pedestal. σ_m contains contributions from the
 255 laser profile as given by Eqn. 1, the transverse size of the positron charge
 256 distribution, σ_e , and the jitter term as defined in section 2.3.2 (σ_{jitter}). A
 257 full treatment of the jitter contribution can be found in [9]. Assuming all
 258 distributions are Gaussian we obtain the following Eqn.:

$$259 \quad \sigma_m = \left[\frac{W_0^2}{4} + \left(\frac{M^2 \lambda (x - x_0)}{2\pi W_0} \right)^2 + \sigma_e^2 + \sigma_{\text{jitter}}^2 \right]^{1/2}, \quad (3)$$

260 where x is the position of the laser focus and x_0 is the location of the positron
 261 bunch, both along the axis of laser propagation.

262 In order to determine x_0 , a number of scans were performed for a range of
 263 values of x , as shown in Fig. 14, and x_0 extracted from a fit to Eqn. 3. Once
 264 the minimum is found, σ_e is extracted from scans taken at $x = x_0$.

265 A similar procedure was performed for the HP as shown in figures 15 and 16.
 266 The extracted positron beam dimensions are $48 \mu\text{m}$ in the vertical and $377 \mu\text{m}$
 267 in the horizontal.

268 4 Conclusion

269 The PETRA LW system has successfully performed horizontal and vertical
 270 beam size measurements.

271 It has successfully employed an automated technique both to find the beam
 272 and to optimize the focus position; this made it possible to perform fast beam

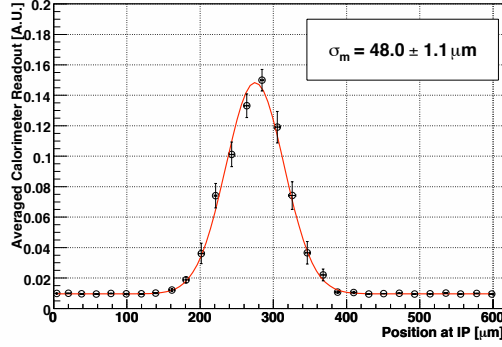


Fig. 13. Vertical scan profile corresponding to the minimum data point of Fig. 14.

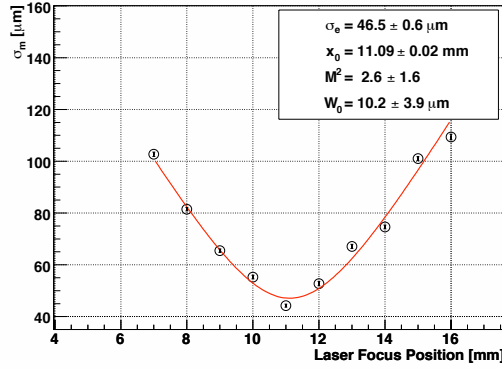


Fig. 14. Plot allowing the extraction of σ_e (from the minimum), M^2 and W_0 in the VP from collision data. The W_0 and M^2 values are in agreement with earlier measurements presented in sections 2.2 and 2.3.1.

measurements in a manner that is non-invasive to normal accelerator operation.

It has performed precision beam size measurements, using a laser spot size of $W_0 \simeq 9 \mu\text{m}$ ($\sigma_0 \simeq 4.5 \mu\text{m}$). Relative vertical positron beam size errors of less than 2.8 % have been achieved in less than 50 s; this could be improved by a higher laser repetition rate.

5 Acknowledgements

We thank the DESY directorate for machine time at PETRA and the PETRA machine crew for their helpful assistance. Work supported by the STFC LC-

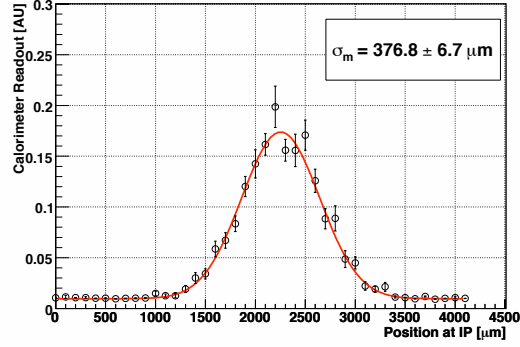


Fig. 15. Horizontal scan profile corresponding to the minimum data point of Fig. 16.

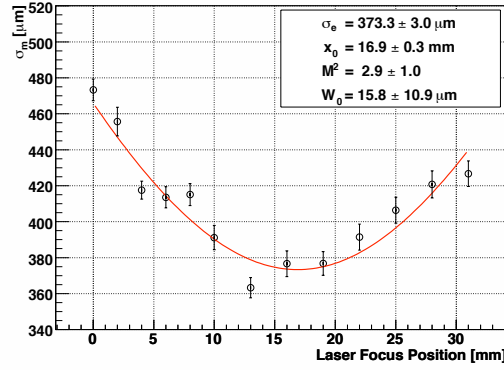


Fig. 16. Plot allowing the extraction of σ_e (from the minimum), M^2 and W_0 in the HP from collision data. The W_0 and M^2 values are in agreement with earlier measurements presented in sections 2.2 and 2.3.1.

282 ABD collaboration, the Royal Society, and the Commission of the European
 283 Communities under the 6th Framework Programme Structuring the European
 284 Research Area, contract number RIDS-RIDS-011899.

285 References

- 286 [1] K.Balewski et al., EPAC 2004, THPKF019 (2004).
- 287 [2] I. Agapov, G. A. Blair, M. Woodley, Phys. Rev. ST Accel. Beams 10, 112801
 288 (2007) Issue 11 November 2007.
- 289 [3] T. Shintake, P. Tenenbaum, Annu. Rev. Nucl. Sci. 49 (1999) 125 162.
- 290 [4] A. Telnov, Nucl. Instrum. Meth. A 513 (2003).

- 291 [5] L. Deacon et. al, PAC07, THOAC01 (2007).
- 292 [6] A. Bosco et al., PAC07, MOPAN110 (2007).
- 293 [7] K.Balewski et al., EPAC 2004 THPLT026 (2004).
- 294 [8] A. Siegman, Lasers, University Science Books, New York, 1990.
- 295 [9] M.T.Price, Laser-Wire Studies for PETRA and the International Linear
296 Collider, University of London thesis, United Kingdom, 2007.
- 297 [10] F.Poirier, Beam Diagnostic Laser-wire and Fast Luminosity Spectrum
298 Measurement at the International Linear Collider, University of London thesis,
299 United Kingdom, 2005.

List of Figures

- | | | |
|---|--|---|
| 1 | Overview of the LW setup. A detailed schematic of the vertical breadboard is shown in Fig. 2. | 3 |
| 2 | Schematic of the LW optical scanning system. The x and y axes are normal to the positron beam trajectory. A close up of the VP scanning system is shown in Fig. 4. | 4 |
| 3 | Photograph of the LW optical scanning system. | 4 |
| 4 | Schematic of the vertical profile scanning system, which contains the piezo-driven mirror and focusing lens. | 5 |
| 5 | Plot of the ABCD matrix calculated beam size from the beam expander to the post IP CCD camera, taking into account the mode quality factor of the laser (M^2). W_0 is the laser spot radius as described in section 2.3.1. | 6 |
| 6 | Laser pulse image taken using CCD profiling equipment in the post IP section of the LW system. | 6 |
| 7 | Oscilloscope trace of the laser pulse as measured by a fast photo-diode (rise time ~ 1 ns) when the laser was unseeded (a) and seeded (b). | 8 |
| 8 | Measurement of M^2 using a $f = 500$ mm lens. The fit equation is given in Eqn. 1. The fit gives $M^2 = 2.68 \pm 0.05$. | 9 |
| 9 | Histograms showing the distribution of laser spot in the horizontal (a) and vertical (b) axes of the digital camera. | 9 |

10	Schematic summarizing the synchronization signals for the LW DAQ.	10
11	The mean peak signal from the PMT is plotted against the electron test-beam energy.	11
12	Schematic of the LW data acquisition system.	12
13	Vertical scan profile corresponding to the minimum data point of Fig. 14.	14
14	Plot allowing the extraction of σ_e (from the minimum), M^2 and W_0 in the VP from collision data. The W_0 and M^2 values are in agreement with earlier measurements presented in sections 2.2 and 2.3.1.	14
15	Horizontal scan profile corresponding to the minimum data point of Fig. 16.	15
16	Plot allowing the extraction of σ_e (from the minimum), M^2 and W_0 in the HP from collision data. The W_0 and M^2 values are in agreement with earlier measurements presented in sections 2.2 and 2.3.1.	15